ZC3H11A mutations cause high myopia by triggering PI3K-AKT and NF-κB mediated signaling pathway in humans and mice

Chong Chen[1,2,3#], Qian Liu[1,2,3#], Cheng Tang[1,2,3], Yu Rong[1,2,3], Xinyi Zhao[1,2,3], Dandan Li[1,2,3], Fan Lu[1,2,3]*, Jia Qu[1,2,3*], Xinting Liu[1,2,3]*

[1]National Engineering Research Center of Ophthalmology and Optometry, Eye Hospital, Wenzhou Medical University, Wenzhou, 325027, China;

[2]National Clinical Research Center for Ocular Diseases, Eye Hospital, Wenzhou Medical University, Wenzhou, 325027, China;

[3]State Key Laboratory of Ophthalmology, Optometry and Visual Science, Eye Hospital, Wenzhou Medical University, Wenzhou, 325027, China.

*For correspondence: liuxt@eye.ac.cn; qujia@eye.ac.cn; lufan62@eye.ac.cn

[#] These authors contributed equally to this work.

Abstract

High myopia (HM) is a severe form of refractive error that results in irreversible visual impairment and even blindness. However, the genetic and pathological mechanisms underlying this condition are not yet fully understood. From a adolescents myopia survey cohort of 1015 HM patients, pathogenic missense mutations were identified in the *ZC3H11A* gene in four patients by whole exome sequencing. This gene is a zinc finger and stress-induced protein that plays a significant role in regulating nuclear mRNA export. To better understand the function and molecular pathogenesis of myopia in relation to gene mutations, a *Zc3h11a* knock-out (KO) mouse model was created. The heterozygous KO (Het-KO) mice exhibited significant shifts in vision towards myopia. Electroretinography revealed that the b-wave amplitude was significantly lower in these mice under dark adaptation. Using immunofluorescence antibodies against specific retinal cell types, the density of bipolar cell-labelled proteins was found to be decreased. Transmission electron microscopy findings suggesting ultrastructural abnormalities of the retina and sclera. Retinal transcriptome sequencing showed that 769 genes were differentially expressed,

and *Zc3h11a* was found to have a negative impact on the PI3K-AKT and NF-κB signaling pathways by quantitative PCR and western blotting. In addition, myopia-related factors, including TGF-β1, MMP-2 and IL-6 were found to be upregulated in the retina or sclera. In summary, this study characterized a new candidate pathogenic gene associated with high myopia, and indicated that the *ZC3H11A* protein may serve as a stress-induced nuclear response trigger, and its abnormality causes disturbances in a series of inflammatory and myopic factors. These findings offer potential therapeutic intervention targets for controlling the development of HM.

Introduction

Myopia is a highly prevalent eye affliction that commonly develops during childhood and early adolescence. The prevalence of myopia among the adult population ranges from 10-30%, while parts of East and Southeast Asia have reported rates as high as 80-90% among young people (Baird et al., 2020; Holden et al., 2016). HM is a severe refractive error characterised by a diopter ≤ -6.00 D or an ocular axis greater than 26 mm. It is estimated that by 2050, the number of people with HM worldwide will reach 938 million, accounting for 9.8% of the total population. HM can trigger a range of adverse ocular changes, such as cataracts, glaucoma, retinal detachment, macular degeneration and possibly total blindness (Koga et al., 2014; Saw et al., 2005). While conventional methods for the prevention and control of myopia can provide some correction, they are not entirely effective in managing its progression, particularly during childhood and adolescence.

With the development of next-generation sequencing, whole exome sequencing (WES) and whole genome sequencing (WGS) have extended the findings of linkage studies to identify potential causes of syndromic HM (sHM) and non-syndromic HM (nsHM). To date, approximately 20 genes with causal associations have been identified in sHM, including *ZNF644*, *SCO2*, *CCDC111*, *LRPAP1*, *SLC39A5*, *LEPREL1*, *P4HA2*, *OPN1LW*, *ARR3*, *BSG*, *NDUFAF7*, *CPSF1*, *TNFRSF21*, *DZIP1*, *XYLT1*, *CTSH*, *GRM6*, *LOXL3* and *GLRA2* (Haarman et al., 2022; Tian et al., 2023; Yang et al., 2023; Ye et al., 2023). These discoveries have provided insight into the molecular

mechanisms underlying HM. However, known candidate genes can only explain about 20% of the causes of this disease (Cai et al., 2019; Tedja et al., 2019). At the same time, the neuromodulators and signal molecules of HM are extremely complex, including sclera extracellular matrix (ECM) remodelling and endoplasmic reticulum (ER) stress (Ikeda et al., 2022), inflammatory responses, the release of dopamine and gamma-aminobutyric acid (GABA), or abnormalities in myopia-related signaling pathways, such as retinoic acid signaling, TGF-β signaling and HIF-1α signaling.

Screening mutations from a adolescents myopia survey cohort by WES, we identified zinc finger CCCH domain-containing protein 11A (*ZC3H11A*) as a HM candidate gene. This particular gene is a member of the zinc finger protein gene family. Several of its members have been linked to myopia or HM, including *ZNF644*, *ZC3H11B*, *ZFP161* and *ZENK*. Like *ZC3H11B*, a gene that is conserved with respect to *ZC3H11A* in humans, the five genome-wide variants loci have previously been found to be strongly associated with greater axial length (AL) or HM (Schippert et al., 2007; Shi et al., 2011; Szczerkowska et al., 2019; Tang et al., 2020; Wang et al., 2004). Recent proteomic studies have indicated that *ZC3H11A* may be a constituent of the transcriptional export (TREX) complex. Additionally, it has been suggested that this protein is involved in stress-induced responses (Younis et al., 2018). Dysfunction of *ZC3H11A* results in enhanced NF-κB signaling through defective IκBα protein expression, which is accompanied by upregulation of numerous innate immune- and inflammation-related mRNAs, including IL-8, IL-6 and TNF in vitro (Jimi et al., 2019). Moreover, patients with myopia have a higher proportion of inflammation-associated cells, including neutrophils, while those with moderate myopia show strained immune system function (Lin et al., 2016; Qi et al., 2022). Conversely, some traditional Chinese medicines can control myopia progression by suppressing AKT and NF-κB mediated inflammatory reactions (Chen et al., 2022). However, the precise pathological mechanism of *ZC3H11A* in myopia development remains unclear, necessitating further research.

The current study identified four HM-related variants in the *ZC3H11A* gene among a cohort of 1015 adolescents. Additionally, KO mice were constructed using the

CRISPR/Cas9 system and their myopic phenotypes, visual function, bipolar cell apoptosis, and retinal and scleral microstructure were assessed. Moreover, RNA sequencing and expression experiment was performed to identify perturbed molecules and pathways and to examine the interactions between these factors in relation to HM. The above results will provide new ideas for the prevention and control of high myopia, especially early-onset, uncorrectable and familial myopia.

Results

ZC3H11A mutations are associated with HM in a Chinese cohort

The subjects were selected from the Myopia Associated Genetics and Intervention Consortium (MAGIC), which is our previously published study involving large-scale high myopia cohorts and genomic sequencing data. Four missense mutations in the *ZC3H11A* gene (c.412G>A, p.V138I; c.128G>A, p.G43E; c.461C>T, p.P154L; and c.2239T>A, p.S747T) were identified in the 1015 HM patients aged from 15 to 18 years. The uncorrected visual acuity (UCVA) and axial length of these patients are presented in Table 1. All of the identified mutations exhibited very low frequencies in the Genome Aggregation Database (gnomAD) and Clinvar, and using pathogenicity prediction software SIFT, PolyPhen2, and CADD, most of them display high pathogenicity levels. Among them, c.412G>A, c.128G>A and c.461C>T were located in or around a domain named zf-CCCH_3 (Figure 1A and B). Furthermore, all of the mutation sites were located in highly conserved amino acids across different species (Figure 1C). Four mutations resulted in a higher degree of conformational flexibility and altered the negative charge at the corresponding sites (Figure 1D and E).

Zc3h11a Het-KO mice exhibited myopic phenotypes

Het-KO mice were constructed at four weeks of age against a C57BL/6J background using CRISPR/Cas9 technology (Supplement Figure 1). Retinal fundus images and ocular histomorphology of *Zc3h11a* Het-KO mice at eight weeks postnatal were assessed against those of their wild-type (WT) counterparts. No significant structural differences were observed (Supplement Figure 2). These findings suggest that the

deletion of *Zc3h11a* does not alter the retinal structure or ocular histomorphology. Therefore, *Zc3h11a* Het-KO mice are a relevant model for the investigation of the role of *Zc3h11a* in refractive development.

Refraction and axial length in *Zc3h11a* Het-KO mice were found to be significantly greater than in WT littermates (independent samples t-test, $p<0.05$; Figure 2A and B). The difference between the two genotypes was statistically significant at weeks 4 and 6. Correspondingly, the vitreous chamber depth of *Zc3h11a* Het-KO mice was deeper than that of WT littermates (independent samples t-test, $p<0.05$; Figure 2C). There were no significant differences in the anterior chamber depth, lens diameter and body weight between the two groups (Figure 2D-F). These results suggest that the Het-KO of the *Zc3h11a* gene may lead to an increase in myopia in mice.

Reduced b-wave amplitude and bipolar cell-labelled protein density in Zc3h11a Het-KO mice

To confirm if *Zc3h11a* is responsible for refractive development regulation, visual function was assessed by electroretinography (ERG). Upon dark adaptation, b-wave amplitudes in seven-week-old Het-KO mice were significantly lower at dark 3.0 and dark 10.0 compared to WT mice (Figure 3A and C). On the contrary, there were no differences in a-wave amplitudes between the Het-KO and WT groups (Figure 3B). Based on the ERG results, variations between Het-KO and WT littermates can be observed. The ERG b-wave, predominantly generated by bipolar cells, was significantly modified in both the 3.0 and 10.0 dark adaptation conditions. Immunofluorescence analyses were performed on frozen retinal sections to investigate this phenomenon further. Specifically, *Zc3h11a*, PKCα, Opsin-1 and Rhodopsin markers were utilised to detect the *Zc3h11a* protein, rod-bipolar cells, cone cells and rod cells, respectively (Figure 3D-F). Additionally, the differences in the *Zc3h11a* and PKCα protein contents of the retina were quantified through western blot analysis. Notably, the protein densities of *Zc3h11a* and PKCα were decreased in the Het-KO group (Figure 3G and H). However, there were no significant differences in the densities of cone and rod cells between the two groups (Figure 3I and J).

Retinal ultrastructure alterations in het-KO mice model

Transmission electron microscopy (TEM) was used to analyse retinal ultrastructure of in 10-week-old mice. In the inner nuclear layer (INL) of the retina, in contrast to WT mice, Het-KO mouse cells had enlarged perinuclear gaps (black arrow), perinuclear cytoplasmic oedema (blue arrow), and thinned and lightened cytoplasm (Figure 4A and B). However, in the outer nuclear layer (ONL), no significant difference in cell morphology was observed between the two groups of mice (Figure 4C and D). Furthermore, when compared to the WT group, the Het-KO mice exhibited relatively damaged photoreceptor cell membrane discs (MB), in which the outer layer was detached and sparsely distributed locally (Figure 4E and F). There were also a small number of broken membrane discs, as well as some disorganized and loosely arranged ones (red arrow), with a slight increase in size (Figure 4G and H).

RNA-Seq analysis of molecular and pathways changes in Zc3h11a Het-KO mice retinas

In the retina transcriptome analysis, 769 genes were differentially expressed (Fold change (FC) of at least two and a P value < 0.05) in the Zc3h11a Het-KO group, of which, 303 were upregulated and 466 were downregulated (Figure 5A and B). GO enrichment analysis revealed that these were primarily involved in biological processes (such as zinc ion transmembrane transport, RNA biosynthetic and metabolic process, and negative regulation of NIK/NF-κb signaling) and molecular functions (such as calcium ion binding and zinc ion transmembrane transporter activity) (Figure 5C and D). KEGG pathway enrichment analysis indicated that the differentially expression genes (DEGs) in the *Zc3h11a* Het-KO group were primarily involved in the PI3K-AKT signaling pathway, MAPK signaling pathway, and neuropsychiatric disease (Figure 5E).

***Zc3h11a* negatively regulates the PI3K-AKT and NF-κB pathways**

PI3K-AKT is one of the most important pathways for cell survival, division,

autophagy and differentiation (Alzahrani, 2019). Meanwhile, it has been found that ZC3H11A can regulate the NF-κB pathway at the level of IκB mRNA export in ZC3-KO cells (Darweesh et al., 2022). IκBα is a critical protein that governs NF-κB function predominantly within the cytoplasmic compartment. It plays a pivotal role in inhibiting the activation of NF-Kb (Dyson and Komives, 2012; Manavalan et al., 2010). In addition, AKT promotes IκBα phosphorylation to undergo degradation, which enhances the nuclear translocation of NF-kB (Alzahrani, 2019; Torrealba et al., 2020). Accordingly, we investigated whether ZC3H11A has any regulatory influence on the transcriptional activation of PI3K-AKT and NF-κB *in vivo*. To this end, we evaluated the mRNA and protein expression levels of ZC3H11A, PI3K, AKT, p-AKT, IκBα and NF-κB in the retina. The expression levels of ZC3H11A, PI3K, AKT, p-AKT and NF-κB were significantly upregulated, while IκBα was downregulated in Het-KO mice (Figure 6A-L). Meanwhile, through transfection of overexpression mutant plasmids, it was found that compared to the wild-type, the mRNA expression levels of IκBα in the nucleus of all four mutant types (ZC3H11A^{V138I}, ZC3H11A^{G43E}, ZC3H11A^{P154L} and ZC3H11A^{S747T}) were significantly reduced (Supplement Figure 3). These findings strongly suggest that ZC3H11A exerts a negative impact on the PI3K-AKT and NF-κB pathways.

TGF-β1, MMP-2 and IL-6 were increased in Zc3h11a Het-KO mice

In animal models of myopia, it has been established that intraocular concentrations of TGF-β1 are elevated (Chen et al., 2013; Liu et al., 2022), especially in the retina and sclera. The abnormal expression of matrix metalloproteinase-2 (MMP-2) and interleukin-6 (IL-6) can induce myopia, and these are regulated by NF-κB (Libermann and Baltimore, 1990; Wu and Schmid-Schönbein, 2011). To investigate the hypothesis that the TGF-β1 and NF-κB signaling pathways exhibit hyperactivity in the retina in the presence of reduced Zc3h11a, we assessed the expression of TGF-β1, MMP-2 and IL-6 at the mRNA levels in the retina and sclera of WT and Het-KO mice, while analysing scleral TEM. Additionally, we confirmed changes in the expression levels of TGF-β1 and MMP-2 in the retina at the protein level. qPCR analysis showed

increased expression of TGF-β1, MMP-2, and IL-6 in the sclera and retina of Het-KO mice compared with WT mice (Figure 7A and B). Scleral TEM results suggested that scleral collagen fibres in Het-KO mice were disorganized over a large area with irregular transverse and longitudinal arrangement (Figure 7C). The western blot results showed increased expression levels of TGF-β1 and MMP-2 in the retinas of *Zc3h11a* Het-KO mice (Figure 7D).

Discussion

This study identified and validated a new candidate gene in a large high myopia cohort, *ZC3H11A*. Moreover, the study provided evidence of the presence of moderate or HM phenotypes and damaged bipolar cells *in vivo* by constructing Het-KO mice for the first time. TEM analysis showed ultrastructural changes in parts of both the retina and sclera of Het-KO mice. To understand how *ZC3H11A* regulates the development of HM, retinal transcriptome sequencing was performed. The results revealed that *Zc3h11a* upregulates the PI3K-AKT and NF-κB signaling pathways. In addition, the expression levels of myopia-related factors, such as TGF-β1, MMP-2 and IL-6, were upregulated in the retina and sclera of the Het-KO mice. Therefore, it can be speculated that the *ZC3H11A* protein may act as a stress-induced nuclear response trigger, its abnormal expression contributing to the early onset of HM.

ZC3H11A is involved in the export and post-transcriptional regulation of selected mRNA transcripts required to maintain metabolic processes in embryonic cells, these are essential for the viability of early mouse embryos (Younis et al., 2023). In studies of chickens, mice and humans, the zinc finger protein *ZENK* was found to play a role in the development of refractive myopic excursion and lengthening of the ocular axis. Moreover, early growth response gene type 1 Egr-1 (the human homolog of *ZENK*) activates the TGF-β1 gene by binding to its promoter, which is thought to be associated with myopia (Baron et al., 2006; Xiao et al., 2022). Another zinc protein finger protein 644 isoform, *ZNF644*, has recently been identified by WES as causing HM in Han Chinese families (Shi et al., 2011). *ZC3H11A* is also a zinc finger protein, and the findings of the current study revealed that *Zc3h11a* Het-KO mice showed a

myopic shift, which is consistent with previous studies reporting reduced protein expression of *Zc3h11a* in an unilateral induced myopic mouse model (Fan et al., 2012).

In vertebrate models, refractive development and ocular axial growth are visually controlled (Wallman and Winawer, 2004). The regulation of axial length or refractive error occurs through complex light-dependent retina-to-sclera signaling (Tkatchenko and Tkatchenko, 2019). Optical scatter information is processed by the retina and then converted into molecular signals that regulate peripheral retinal growth and scleral connective tissue renewal, ultimately affecting the growth rate of the posterior segment of the eye (Harper and Summers, 2015; Tkatchenko et al., 2006; Tkatchenko et al., 2018). All cell types of the retina contain myopia-related genes and retinal circuitry driving refractive error. In this study, Het-KO mice were found to have reduced b-wave amplitudes, diminished relative fluorescence intensity of bipolar cells and ultrastructural changes in inner nuclear layer (INL) of the retina. Therefore, it is presumed that retinal circuitry changes result in impairment of visual signal processing and transduction causing HM.

Aberrant activation of the PI3K-AKT and NF-κB signaling pathways has been identified in highly myopic retinas. Following the sequencing evidence indicating elevations in PI3K-AKT and NF-κB signaling (Lin et al., 2016), we sought to explore the potential interplay between these pathways in mice. The results revealed that a decrease in *Zc3h11a* inhibited the translocation of IκBα from the nucleus to the cytoplasm. IκBα is a downstream factor of PI3K-AKT and binds to NF-κB (p65) in the cytoplasm, inhibiting its nuclear translocation. The qPCR and western Blot results verified that *Zc3h11a* negatively regulates both the PI3K-AKT and NF-κB signaling pathways. Thus, *Zc3h11a* may exert an influence on these pathways by modulating the cytoplasmic levels of IκBα, contributing to the development of myopia.

NF-κB was first discovered 25 years ago and described as a key regulator of induced gene expression in the immune system, playing a central role in the coordinated control of intrinsic immune and inflammatory responses (Hayden and Ghosh, 2011; Morgan and Liu, 2011). The downstream factors of this pathway include IL-6, IL-8,

TNF-α, MMP-2, TGF-β1, etc (Jimi et al., 2019; Yoshida and Whitsett, 2006). Studies have demonstrated that the MMP-2 and IL-6 expression levels are increased in myopic eyes and that inhibiting MMP-2 or IL-6 expression will provide some degree of control over myopia progression (Lin et al., 2016; Zhao et al., 2018). Identification of the PI3K-AKT-NF-κB signaling pathway and downstream myopia effect in our study may open up new opportunities for the prevention and treatment of HM and fundus lesions in the future.

There are a number of limitations of this study that should be acknowledged. First, the patient's ophthalmic examination was not comprehensive enough, and genetic analysis such as segregation analysis was not performed. Second, Zc3h11a homozygous KO (Homo-KO) mice were not obtained in our study because homozygous deletion of exons may confer embryonic lethality (Younis et al., 2023). Third, while the current study observed a reduced b-wave amplitude and bipolar cell fluorescence staining intensity in Het-KO mice, an in-depth exploration of the underlying mechanism was beyond the scope of the research. Finally, there was a limited observation time in this study and the effect of *ZC3H11A* on the late refractive system was not assessed.

Overall, this study has provided four key findings. First, it was confirmed that the *ZC3H11A* is a new candidate gene associated with HM in a cohort of Chinese Han individuals. Secondly, changes in *Zc3h11a* expression were found to affect retinal function, particularly in bipolar cells. Third, changes in *Zc3h11a* expression were found to cause alterations in numerous signaling pathways, the most notable being the PI3K-AKT and NF-κB pathways. Fourth, changes in *Zc3h11a* expression were found to cause changes in the myopia-related genes TGF-β1, MMP-2 and IL-6. The above results suggest that abnormal expression of *Zc3h11a* triggers nuclear translocation defects of IκBα, thereby exerting negative feedback regulation of the PI3K-AKT signaling pathway and inhibiting the NF-κB signaling pathway. At the same time, the increase in TGF-β1 in myopic eyes stimulates the PI3K-AKT signaling pathway, which leads to activation of the PI3K-AKT signaling pathway, resulting in downstream degradation of IκBα after phosphorylation. This, in turn, increases the

nuclear translocation of NF-κB. To sum up, *Zc3h11a* promotes the myopia-associated factor TGF-β1 by acting directly or indirectly on both the PI3K-AKT and NF-κB signaling pathway-mediated stress reactions and the expression of MMP-2 and IL-6, which together, promote the development of early high myopia (Figure 8). Therefore, this model can be used as one of the new strategies for intervention and treatment of high myopia. However, because the causes of myopia or HM are complex and involve different tissues and molecular pathways in the eye, it is likely that future research will identify more genes and molecular mechanisms that could provide guidance for clinical intervention and treatment.

Materials and methods

Ethics approval and consent to participate

The studies that involved human participants were approved by the Eye Hospital, Wenzhou Medical University (Wenzhou, China), and were carried out in strict adherence to the guidelines of the Helsinki Declaration. All participants provided informed consent. Furthermore, all animal experiments were approved by the Animal Care and Ethics Committee at Wenzhou Medical University and were performed according to the guidelines set forth in the Association for Research in Vision and Ophthalmology Statement for the Use of Animals in Ophthalmic and Visual Research. (https://www.arvo.org/About/policies/statement-for-the-use-of-animals-in-ophthalmic-and-vision-research/).

Recruitment of subjects

A total of 1015 sporadic HM patients (aged from 15-18) were recruited from the Eye Hospital of Wenzhou Medical University for MAGIC project (Su et al., 2023). HM was defined as SE ≤ -6.00 D in either eye (Flitcroft et al., 2019). Some patients underwent certain ophthalmic examinations, including visual acuity (at least three measurements under non-cycloplegia), axial length and fundus photography were performed.

WES and the detection of variants

DNA was extracted from all probands using a FlexiGene DNA Kit (Qiagen, Venlo, The Netherlands), according to the manufacturer's protocol. DNA from all probands underwent WES using a Twist Human Core Exome Kit and an Illumina NovaSeq 6000 sequencing system (150PE) (Berry Genomics Institute, Beijing, China). The mean depth and coverage of the target region were approximately 78.26× and 99.7%, respectively. Sequence reads were aligned to the reference human genome (UCSC hg19) using the Burrows-Wheeler aligner (BWA). The variants were called and annotated with Verita Trekker and Enliven software (Transcript ID, ENST00000332127.4, Berrry Genomics Institute), respectively.

Het-KO mice model construction, husbandry and ocular biometric measurements

Het-KO mice were constructed at four weeks of age against a C57BL/6J background using CRISPR/Cas9 technology at GemPharmatech Co.,Ltd (Nanjing, China). Exon5-exon6 of the *Zc3h11a* transcript was recommended as the KO region; this region contains a 244bp coding sequence. Littermates of Het-KO and WT mice were used for all experiments. All animals were housed in the animal husbandry room of Wenzhou Medical University. Mice were housed in standard transparent mouse cages at 22±2°C with a 12-hour light/12-hour dark cycle (light from 8 am to 8 pm, brightness approximately 200-300 lux) and free access to food and water. To exclude the effect of ocular developmental malformations, mice with small eyes and ocular lesions were excluded from the observation cohort. Body weight, refraction and ocular biometrics of Het-KO (n=14) and WT (n=10) mice were assessed at 4, 5, 6, 8 and 10 weeks of age.

Electroretinography

To evaluate the effect of *Zc3h11a* on the electrophysiological properties of various neuronal populations in the retina, ERG was performed on the right eye of Het-KO and WT littermates at seven weeks of age, at the same time of day (n=12). Both

scotopic and photopic ERG responses were evaluated. The mice were dark-adapted overnight, and all procedures were performed under dim red light (<1 lux). The animals were anaesthetized with intraperitoneal injection of pentobarbital sodium (40 mg/kg) and the pupils were dilated with 0.5% tropicamide. A heating table (37□) was used to maintain body temperature. ERG was recorded using a Roland Electrophysiological System (RETI-Port21, Roland Consult, Germany) with ring-shaped corneal electrodes. Three light intensities (0.01, 3.0 and 10.0 cds/m^2) were applied to each animal. The following parameters were measured: a-wave amplitude and b-wave amplitude. Photopic ERG was measured at a light intensity of 3.0 cds/m^2 after 10 min light adaption at 25 cds/m^2. The responses of the Het-KO eyes (right) were compared with those of the WT eyes (right).

Immunofluorescence

Whole mouse eyes (10 weeks, littermates Het-KO and WT) were fixed with 4% para-formaldehyde (BL539A, Biosharp, China) for 1 h and 30% sucrose for dehydration overnight. Then, they were fabric-embedded in a frozen fabric matrix compound at -20□. Prepared tissue blocks were segmented with a cryostat at a thickness of 12 microns and collected on clean adhesive slides. The slices containing the sections were air-dried at room temperature (RT) for 15 min. After washing 3× with 1× PBS for 5 min, 5% BSA (SW3015, Solarbio, China) and 0.03% triton-X100 (P0096, Beyotime, China) diluted with 1× PBS were added as permeable membrane-blocking buffers. The slides were incubated for 1 h at RT in a humid chamber. Then, they were incubated overnight at 4□ with the specific primary antibody Zc3h11a (1:50, 26081, Proteintech, USA). PKC α (1:200, ab32518, Abcam, UK), Opsin-1 (1:200, NB110-74730, Novus Biologicals, USA) and Rhodopsin (1:200, NBP2-25160, Novus Biologicals, USA) were added and the slices were incubated further at 4□ in a humid chamber overnight. After washing 4× with 1× PBS for 6 min, goat anti-rabbit Alexa Fluor 488 (1:500, ab150077, Abcam, UK) was added and the slides were incubated for 90 min at RT. After washing, the slides were mounted with an antifade medium containing DAPI (P0131, Beyotime, China) to visualize the cell nucleus. Sections

incubated with 5% BSA and without primary antibodies were used as negative controls. A fluorescence microscope (LSM 880, ZEISS, Germany) was used to examine the slides and capture images. The experiments were repeated in duplicate with three different samples.

Transmission electron microscopy

At 10 weeks of age, two mice of each genotype were euthanized, and their eyes were removed. The eyes were fixed in a solution containing 2.5% glutaraldehyde and 0.01 M phosphate buffer (PB) (pH 7.0-7.5) for 15 min while the optic cups were dissected. The optic cups were then fixed with 1% osmium acid at room temperature away from light for 2h, after which they were rinsed three times with 0.1 MPB for 15min each time. Tissues were sequentially dehydrated in 30%-50%-70%-80%-95%-100%-100% ethanol upstream for 20 min each time, and 100% acetone twice for 15 min each time. Finally, the tissues were embedded in epoxy resin (Polybed 812) mixed 1:1 with acetone. Ultrathin sections were prepared using diamond knives and an EM UC7 ultramicrotome (Leica, Germany), then the sections were stained with 2% aqueous dioxygen acetate and 1% phosphotungstic acid (pH 3.2). Finally, the structures were examined using a transmission electron microscope (HT7700, Hitachi, Tokyo, Japan).

Cell culture, plasmid construction and transfected

HEK293T cell line (from Chinese Academy of Sciences) was cultured in DMEM medium containing 10% high-quality 10% fetal bovine serum (FBS) and 1% penicillin streptomycin dual antibody. Using restriction endonucleases HindIII and EcoRI to cleave the target gene product (wild type, ZC3H11A^{V138I}, ZC3H11A^{G43E}, ZC3H11A^{P154L} and ZC3H11A^{S747T}) and vector pcDNA3.1 (+), and purify the fragments. Then, under the action of T4 DNA ligase, the target gene was ligated with the vector pcDNA3.1 (+), and the ligated product was transformed into competent bacterial cells. Sequencing was used to identify and select the successfully constructed target gene expression plasmid vector. Finally, a sufficient amount of vector plasmids were obtained through ultrapure endotoxin extraction. Transfected

with wild type, ZC3H11A^{V138I}, ZC3H11A^{G43E}, ZC3H11A^{P154L} and ZC3H11A^{S747T} overexpression plasmids using NDE3000 reagent (Western, China).

RNA sequencing analysis of molecular and pathway changes in the mouse retina

Mice aged four weeks were executed by cervical dislocation after CO_2 asphyxiation. Then, the eyes were enucleated and dissected to obtain the entire retinas. Three eye retinas from the *Zc3h11a* Het-KO and WT groups were used for the mRNA sequencing experiments and performed by Biomarker Biotechnology Co. (Beijing, China). The mRNA sequences were mapped to the genome (GRCm38). WebGestalt (http://www.webgestalt.org/) was used to generate GO terms and KEGG pathways.

RNA extraction and qRT-PCR

To determine the reliability of the transcriptome results, qPCR validation was performed. Total RNA and nuclear RNA were extracted using Trizol reagent (RC112, Vazyme, China) and Cytodynamic & Nuclear RNA Purification Kit (21000, Norgen Biotek, Canada), respectively, and the purity was confirmed by the OD260/280 nm absorption ratio (1.9-2.1) (Nanodrop 2000, Thermo Scientific, USA). Total RNA (2 μg) was reverse transcribed to cDNA using a cDNA Synthesis Kit (R323, Vazyme, China). qPCR was performed with a RT-PCR detection system (Applied Biosystems, California, USA) using a SYBR Premix Ex Taq Kit (Q711, Vazyme, China), according to the manufacturer's instructions. qRT-PCR was performed (ABI-Q6, California, USA) in a 20 μL reaction, under the following conditions: 95°C for 10 min, followed by 40 cycles of amplification at 95°C for 10 s and 60°C for 60 s. Melting curve analysis was used to determine specific amplification. All experiments were performed in triplicate. Relative quantification was performed using the ΔΔCt method. The specific gene products were amplified using the following primer pairs (Supplement Table 1).

Western blot

The mouse retina was separated immediately after enucleation of the eyeball and

lysed in RIPA (10 mM Tris-Cl, 100 mM NaCl, 1 mM EDTA, 1 mM NaF, 20 mM $Na_4P_2O_7$, 2 mM Na_3VO_4, 1% Triton X-100, 10% glycerol, 0.1% sodium dodecyl sulphate and 0.5% deoxycholate) lysis buffer containing protease and phosphatase inhibitors (P1045, Beyotime, China). Equal amounts of protein (15 μg) were separated on 10% Tris-glycine gel, transferred to PVDF (polyvinylidene fluoride) membranes, and blocked with 5% skim milk. The primary antibodies used included ZC3H11A (ab99930, Abcam, UK), AKT (#4691, Cell Signaling Technology, USA), p-AKT (#4060, Cell Signaling Technology, USA), IκBα (ab32518, Abcam, UK), NF-κB (ab32536, Abcam, UK), TGF-β1 (21898, Proteintech, USA) and MMP-2 (ab92536, Abcam, UK) diluted to 1:1000 in TBST-5% milk. Then, the membranes were incubated with goat anti-rabbit IgG conjugated with HRP (1:2000 in TBST-5% milk) (SA00001-2, Proteintech, USA) for 90 min at room temperature and developed using western blotting reagents (BL523B, Bioshark, China). GAPDH (AF2823, Byotime, China) was used as the internal control.

Software and statistical analysis

All experiments were repeated at least once, and sample sizes and reported results reflect the cumulative data for all trials of each experiment. Each result is expressed as the mean ± standard deviation (SD). Pearson's test was used to assess the normality of the data. The normally distributed data were subjected to parametric analyses. Unpaired Student's t-tests were used for parametric analyses between two groups. Data that were not normally distributed or had a sample size that was too small, were subjected to nonparametric analyses. Nonparametric tests between two groups were performed using the Wilcoxon signed-rank test for matched pairs, the Mann-Whitney U-test or the Kruskal-Wallis test for multiple comparisons (GraphPad Prism 9, La Jolla, CA). A difference was considered statistically significant when the p-value was less than 0.05 and highly significant if it was less than 0.01 or less than 0.001.

Acknowledgements

The authors wish to thank all of the members of our lab. Additionally, we thank myopia research group at Eye Hospital of Wenzhou Medical University for their technical assistance.

Additional information

Funding

This work was supported by the National Natural Science Foundation of China (82101176), the Natural Science Foundation of Zhejiang Province (LTGD23H120002), the Health Technology Plan Project in Zhejiang Province (2021KY151) and the Science and Technology Project of Wenzhou (Y20220774)

Author Contributions

Conceptualisation, Xinting Liu, Jia Qu and Fan Lu; methodology, Chong Chen and Qian Liu; data analysis, Chong Chen, Qian Liu, Cheng Tang and Yu Rong; investigation and cohort construction, Xinting Liu, Jia Qu, Fan Lu, Dandan Li and Xinyi Zhao; writing original draft preparation, Chong Chen, Qian Liu and Xinting Liu; writing-review and editing, Xinting Liu, Jia Qu and Fan Lu; funding acquisition, Xinting Liu, Jia Qu and Fan Lu. All authors have read and agreed to the published version of the manuscript.

Ethics approval

The study was approved by the Institutional Review Board of Eye Hospital, Wenzhou Medical University, Zhejiang, China (REC reference 2021-015-K-12-01). Informed consent was obtained from each subject. The study was approved by the Animal Care and Ethics Committee at Wenzhou Medical University (Wenzhou, China).

Data availability

All data generated or analysed during this study are included in the manuscript and supporting files.

References

Alzahrani, A.S., 2019. PI3K/Akt/mTOR inhibitors in cancer: At the bench and bedside. Semin Cancer Biol 59, 125-132.

Baird, P.N., Saw, S.M., Lanca, C., Guggenheim, J.A., Smith Iii, E.L., Zhou, X., Matsui, K.O., Wu, P.C., Sankaridurg, P., Chia, A., Rosman, M., Lamoureux, E.L., Man, R., He, M., 2020. Myopia. Nat Rev Dis Primers 6, 99.

Baron, V., Adamson, E.D., Calogero, A., Ragona, G., Mercola, D., 2006. The transcription factor Egr1 is a direct regulator of multiple tumor suppressors including TGFbeta1, PTEN, p53, and fibronectin. Cancer Gene Ther 13, 115-124.

Cai, X.-B., Zheng, Y.-H., Chen, D.-F., Zhou, F.-Y., Xia, L.-Q., Wen, X.-R., Yuan, Y.-M., Han, F., Piao, S.-Y., Zhuang, W., Lu, F., Qu, J., Yu, A.Y., Jin, Z.-B., 2019. Expanding the Phenotypic and Genotypic Landscape of Nonsyndromic High Myopia: A Cross-Sectional Study in 731 Chinese Patients. Invest Ophthalmol Vis Sci 60, 4052-4062.

Chen, B.-Y., Wang, C.-Y., Chen, W.-Y., Ma, J.-X., 2013. Altered TGF-β2 and bFGF expression in scleral desmocytes from an experimentally-induced myopia guinea pig model. Graefes Arch Clin Exp Ophthalmol 251, 1133-1144.

Chen, C.-S., Hsu, Y.-A., Lin, C.-H., Wang, Y.-C., Lin, E.-S., Chang, C.-Y., Chen, J.J.-Y., Wu, M.-Y., Lin, H.-J., Wan, L., 2022. Fallopia Japonica and Prunella vulgaris inhibit myopia progression by suppressing AKT and NFκB mediated inflammatory reactions. BMC Complement Med Ther 22, 271.

Darweesh, M., Younis, S., Hajikhezri, Z., Ali, A., Jin, C., Punga, T., Gupta, S., Essand, M., Andersson, L., Akusjärvi, G., 2022. ZC3H11A loss of function enhances NF-κB signaling through defective IκBα protein expression. Front Immunol 13, 1002823.

Dyson, H.J., Komives, E.A., 2012. Role of disorder in IκB-NFκB interaction. IUBMB Life 64, 499-505.

Fan, Q., Barathi, V.A., Cheng, C.-Y., Zhou, X., Meguro, A., Nakata, I., Khor, C.-C., Goh, L.-K., Li, Y.-J., Lim, W.e., Ho, C.E.H., Hawthorne, F., Zheng, Y., Chua, D., Inoko, H., Yamashiro, K., Ohno-Matsui, K., Matsuo, K., Matsuda, F., Vithana, E., Seielstad, M., Mizuki, N., Beuerman, R.W., Tai, E.S., Yoshimura, N., Aung, T., Young,

T.L., Wong, T.-Y., Teo, Y.-Y., Saw, S.-M., 2012. Genetic variants on chromosome 1q41 influence ocular axial length and high myopia. PLoS Genet 8, e1002753.

Flitcroft, D.I., He, M., Jonas, J.B., Jong, M., Naidoo, K., Ohno-Matsui, K., Rahi, J., Resnikoff, S., Vitale, S., Yannuzzi, L., 2019. IMI - Defining and Classifying Myopia: A Proposed Set of Standards for Clinical and Epidemiologic Studies. Invest Ophthalmol Vis Sci 60, M20-M30.

Haarman, A.E.G., Thiadens, A.A.H.J., van Tienhoven, M., Loudon, S.E., de Klein, J.E.M.M.A., Brosens, E., Polling, J.R., van der Schoot, V., Bouman, A., Kievit, A.J.A., Hoefsloot, L.H., Klaver, C.C.W., Verhoeven, V.J.M., 2022. Whole exome sequencing of known eye genes reveals genetic causes for high myopia. Hum Mol Genet 31, 3290-3298.

Harper, A.R., Summers, J.A., 2015. The dynamic sclera: extracellular matrix remodeling in normal ocular growth and myopia development. Exp Eye Res 133, 100-111.

Hayden, M.S., Ghosh, S., 2011. NF-κB in immunobiology. Cell Res 21, 223-244.

Holden, B.A., Fricke, T.R., Wilson, D.A., Jong, M., Naidoo, K.S., Sankaridurg, P., Wong, T.Y., Naduvilath, T.J., Resnikoff, S., 2016. Global Prevalence of Myopia and High Myopia and Temporal Trends from 2000 through 2050. Ophthalmology 123, 1036-1042.

Ikeda, S.-I., Kurihara, T., Jiang, X., Miwa, Y., Lee, D., Serizawa, N., Jeong, H., Mori, K., Katada, Y., Kunimi, H., Ozawa, N., Shoda, C., Ibuki, M., Negishi, K., Torii, H., Tsubota, K., 2022. Scleral PERK and ATF6 as targets of myopic axial elongation of mouse eyes. Nat Commun 13, 5859.

Jimi, E., Fei, H., Nakatomi, C., 2019. NF-κB Signaling Regulates Physiological and Pathological Chondrogenesis. Int J Mol Sci 20.

Koga, M., Mizuno, Y., Watanabe, I., Kawakami, H., Goto, T., 2014. Role of VPAC2 receptor in monocrotaline-induced pulmonary hypertension in rats. J Appl Physiol (1985) 117, 383-391.

Libermann, T.A., Baltimore, D., 1990. Activation of interleukin-6 gene expression through the NF-kappa B transcription factor. Mol Cell Biol 10, 2327-2334.

Lin, H.-J., Wei, C.-C., Chang, C.-Y., Chen, T.-H., Hsu, Y.-A., Hsieh, Y.-C., Chen, H.-J., Wan, L., 2016. Role of Chronic Inflammation in Myopia Progression: Clinical Evidence and Experimental Validation. EBioMedicine 10, 269-281.

Liu, S., Chen, T., Chen, B., Liu, Y., Lu, X., Li, J., 2022. Lrpap1 deficiency leads to myopia through TGF-β-induced apoptosis in zebrafish. Cell Commun Signal 20, 162.

Manavalan, B., Basith, S., Choi, Y.-M., Lee, G., Choi, S., 2010. Structure-function relationship of cytoplasmic and nuclear IκB proteins: an in silico analysis. PLoS One 5, e15782.

Morgan, M.J., Liu, Z.-g., 2011. Crosstalk of reactive oxygen species and NF-κB signaling. Cell Res 21, 103-115.

Qi, J., Pan, W., Peng, T., Zeng, L., Li, X., Chen, Z., Yang, Z., Xu, H., 2022. Higher Circulating Levels of Neutrophils and Basophils Are Linked to Myopic Retinopathy. Int J Mol Sci 24.

Saw, S.-M., Gazzard, G., Shih-Yen, E.C., Chua, W.-H., 2005. Myopia and associated pathological complications. Ophthalmic Physiol Opt 25, 381-391.

Schippert, R., Burkhardt, E., Feldkaemper, M., Schaeffel, F., 2007. Relative axial myopia in Egr-1 (ZENK) knockout mice. Invest Ophthalmol Vis Sci 48, 11-17.

Shi, Y., Li, Y., Zhang, D., Zhang, H., Li, Y., Lu, F., Liu, X., He, F., Gong, B., Cai, L., Li, R., Liao, S., Ma, S., Lin, H., Cheng, J., Zheng, H., Shan, Y., Chen, B., Hu, J., Jin, X., Zhao, P., Chen, Y., Zhang, Y., Lin, Y., Li, X., Fan, Y., Yang, H., Wang, J., Yang, Z., 2011. Exome sequencing identifies ZNF644 mutations in high myopia. PLoS Genet 7, e1002084.

Su, J., Yuan, J., Xu, L., Xing, S., Sun, M., Yao, Y., Ma, Y., Chen, F., Jiang, L., Li, K., Yu, X., Xue, Z., Zhang, Y., Fan, D., Zhang, Y., Liu, H., Liu, X., Zhang, G., Wang, H., Zhou, M., Lyu, F., An, G., Yu, X., Myopia Associated Genetics and Intervention Consortium., Xue, Y., Yang, J., QU, J., 2023. Sequencing of 19,219 exomes identifies a low-frequency variant in FKBP5 promoter predisposing to high myopia in a Han Chinese population. Cell Rep 42, 112510.

Szczerkowska, K.I., Petrezselyova, S., Lindovsky, J., Palkova, M., Dvorak, J., Makovicky, P., Fang, M., Jiang, C., Chen, L., Shi, M., Liu, X., Zhang, J., Kubik-

Zahorodna, A., Schuster, B., Beck, I.M., Novosadova, V., Prochazka, J., Sedlacek, R., 2019. Myopia disease mouse models: a missense point mutation (S673G) and a protein-truncating mutation of the Zfp644 mimic human disease phenotype. Cell Biosci 9, 21.

Tang, S.M., Li, F.F., Lu, S.Y., Kam, K.W., Tam, P.O.S., Tham, C.C., Pang, C.P., Yam, J.C.S., Chen, L.J., 2020. Association of the ZC3H11B, ZFHX1B and SNTB1 genes with myopia of different severities. Br J Ophthalmol 104, 1472-1476.

Tedja, M.S., Haarman, A.E.G., Meester-Smoor, M.A., Kaprio, J., Mackey, D.A., Guggenheim, J.A., Hammond, C.J., Verhoeven, V.J.M., Klaver, C.C.W., 2019. IMI - Myopia Genetics Report. Invest Ophthalmol Vis Sci 60.

Tian, Q., Tong, P., Chen, G., Deng, M., Cai, T.e., Tian, R., Zhang, Z., Xia, K., Hu, Z., 2023. GLRA2 gene mutations cause high myopia in humans and mice. J Med Genet 60, 193-203.

Tkatchenko, A.V., Walsh, P.A., Tkatchenko, T.V., Gustincich, S., Raviola, E., 2006. Form deprivation modulates retinal neurogenesis in primate experimental myopia. Proc Natl Acad Sci U S A 103, 4681-4686.

Tkatchenko, T.V., Tkatchenko, A.V., 2019. Pharmacogenomic Approach to Antimyopia Drug Development: Pathways Lead the Way. Trends Pharmacol Sci 40, 833-852.

Tkatchenko, T.V., Troilo, D., Benavente-Perez, A., Tkatchenko, A.V., 2018. Gene expression in response to optical defocus of opposite signs reveals bidirectional mechanism of visually guided eye growth. PLoS Biol 16, e2006021.

Torrealba, N., Vera, R., Fraile, B., Martínez-Onsurbe, P., Paniagua, R., Royuela, M., 2020. TGF-β/PI3K/AKT/mTOR/NF-kB pathway. Clinicopathological features in prostate cancer. Aging Male 23, 801-811.

Wallman, J., Winawer, J., 2004. Homeostasis of eye growth and the question of myopia. Neuron 43, 447-468.

Wang, G.-B., Zhang, Q.-J., Xiao, X.-S., Li, J.-Z., Zhang, F.-S., Li, S.-Q., Li, W., Li, T., Jia, X.-Y., Guo, L., Guo, X.-M., 2004. [Variations of the zinc finger protein 161 gene in Chinese with or without high myopia]. Yi Chuan 26, 155-159.

Wu, K.-I.S., Schmid-Schönbein, G.W., 2011. Nuclear factor kappa B and matrix metalloproteinase induced receptor cleavage in the spontaneously hypertensive rat. Hypertension 57, 261-268.

Xiao, Q., Xiao, J., Liu, J., Liu, J., Shu, G., Yin, G., 2022. Metformin suppresses the growth of colorectal cancer by targeting INHBA to inhibit TGF-β/PI3K/AKT signaling transduction. Cell Death Dis 13, 202.

Yang, E., Yu, J., Liu, X., Chu, H., Li, L., 2023. Familial Whole Exome Sequencing Study of 30 Families With Early-Onset High Myopia. Invest Ophthalmol Vis Sci 64, 10.

Ye, M., Ma, Y., Qin, Y.-X., Cai, B., Ma, L.-M., Ma, Z., Liu, Y., Jin, Z.-B., Zhuang, W.-J., 2023. Mutational investigation of 17 causative genes in a cohort of 113 families with nonsyndromic early-onset high myopia in northwestern China. Mol Genet Genomics 298, 669-682.

Yoshida, M., Whitsett, J.A., 2006. Alveolar macrophages and emphysema in surfactant protein-D-deficient mice. Respirology 11 Suppl, S37-S40.

Younis, S., Jouneau, A., Larsson, M., Oudin, J.F., Adenot, P., Omar, J., Brochard, V., Andersson, L., 2023. Ablation of ZC3H11A causes early embryonic lethality and dysregulation of metabolic processes. Proc Natl Acad Sci U S A 120, e2216799120.

Younis, S., Kamel, W., Falkeborn, T., Wang, H., Yu, D., Daniels, R., Essand, M., Hinkula, J., Akusjärvi, G., Andersson, L., 2018. Multiple nuclear-replicating viruses require the stress-induced protein ZC3H11A for efficient growth. Proc Natl Acad Sci U S A 115, E3808-E3816.

Zhao, F., Zhou, Q., Reinach, P.S., Yang, J., Ma, L., Wang, X., Wen, Y., Srinivasalu, N., Qu, J., Zhou, X., 2018. Cause and Effect Relationship between Changes in Scleral Matrix Metallopeptidase-2 Expression and Myopia Development in Mice. Am J Pathol 188, 1754-1767.

Table 1 The clinical features and mutations of affected patients

Patient information			Refraction (D)		Axial length (mm)		Variation information			Prediction software and databases				
ID.	Sex	Age	OD	OS	OD	OS	Genotype	chromosomal positions	Existing_variation (rs numbers)	SIFT (score)	PolyPhen2 (score)	CADD (score)	gnomAD	Clinvar
1	M	18	-6.50	-5.125	25.68	25.34	c.412G>A:p.Val138Ile, Het	chr1:203798692-203798692	rs142418357	D (0.03)	PB (0.912)	24.3	7.95E-06	-
2	F	15	-4.25	-6.125	24.61	25.11	c.128G>A:p.Gly43Glu, Het	chr1:203787771-203787771	-	D (0)	PS (0.906)	26	-	-
3	M	17	-8.00	-8.75	26.16	27.02	c.461C>T :p.Pro154Leu, Het	chr1:203798741-203798741	-	D (0)	PS (0.628)	29.3	-	-
4	F	15	-6.25	-3.70	25.53	24.86	c.2239T>A:p.Ser747Thr, Het	chr1:203821333-203821333	-	T (0.1)	PS (0.838)	22.7	-	-

M, male; F, female; Het, heterozygote; OD, ocular dexter; OS, oculus sinister; D, deleterious, T, tolerated; PB, probably_damaging; PS, possibly_damaging; gnomAD, Genome Aggregation Database; AF, Allele Frequency; -, Not Applicable

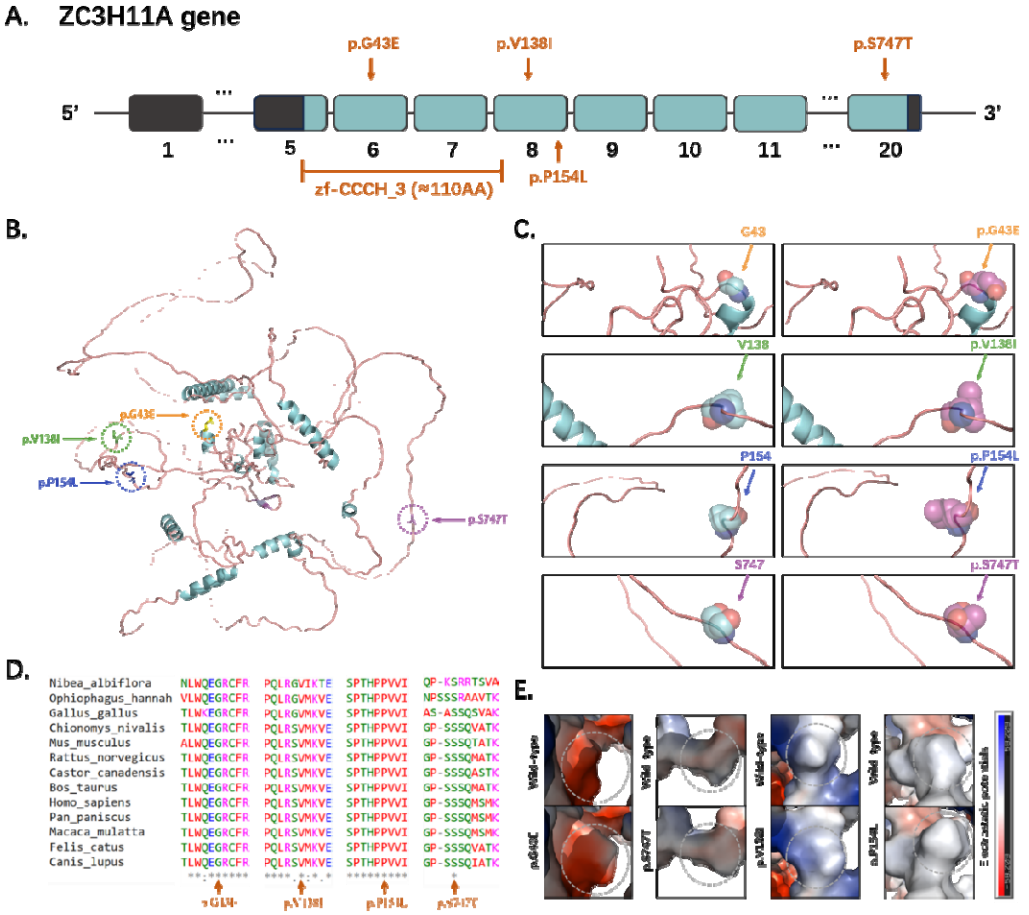

Figure 1. Structural modelling of ZC3H11A gene mutations. (A) Illustration of exons and mutation sites of ZC3H11A; exons 5-8 of ZC3H11A encode the zf-CCCH_3 protein domain. (B) A structural model of the full-length human ZC3H11A protein was generated using PyMOL; the locations of the four mutation sites are marked. (C) The p.G43E mutation is located in exon 6, while the p.V138I and p.P154L mutations are in exon 8, and the p.S747T mutation is in exon 20. (D) Multiple sequence alignment of the proteins where ZC3H11A mutations are found in multiple species. (E) These mutations can result in a higher degree of conformational flexibility at the corresponding sites, potentially destabilizing the structural domain.

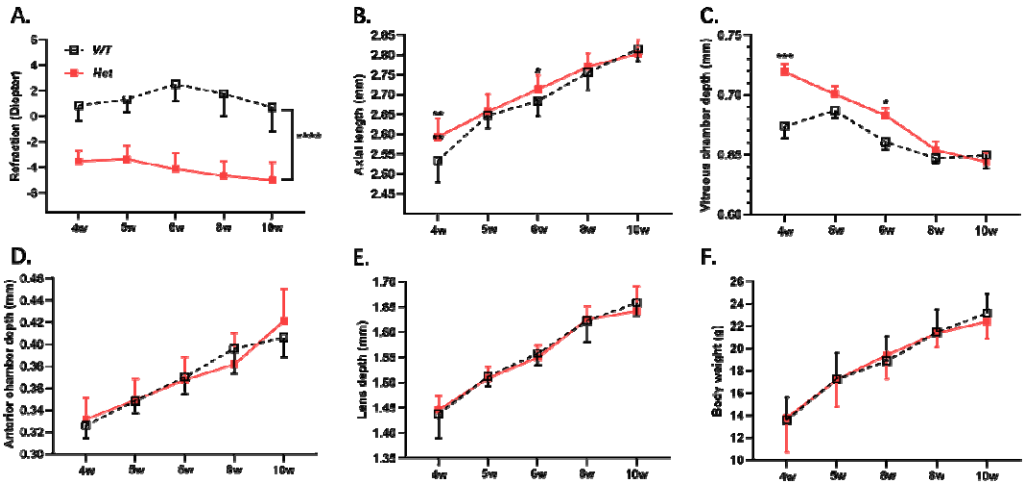

Figure 2. Comparison of ocular biometrics and body weights of Zc3h11a Het-KO (n=14) and WT (n=10) littermates during weeks 4-10 of development. (A, B) Refraction and axial length in Zc3h11a Het-KO mice. (C) Vitreous chamber depth. (D-F) Anterior chamber depth, lens depth and body weight. The effect of genotype on time-dependent refractive development was assessed through independent samples t-tests. P-values are indicated as follows: *P<0.05, **P<0.01, ***P<0.001 and ****<0.0001.

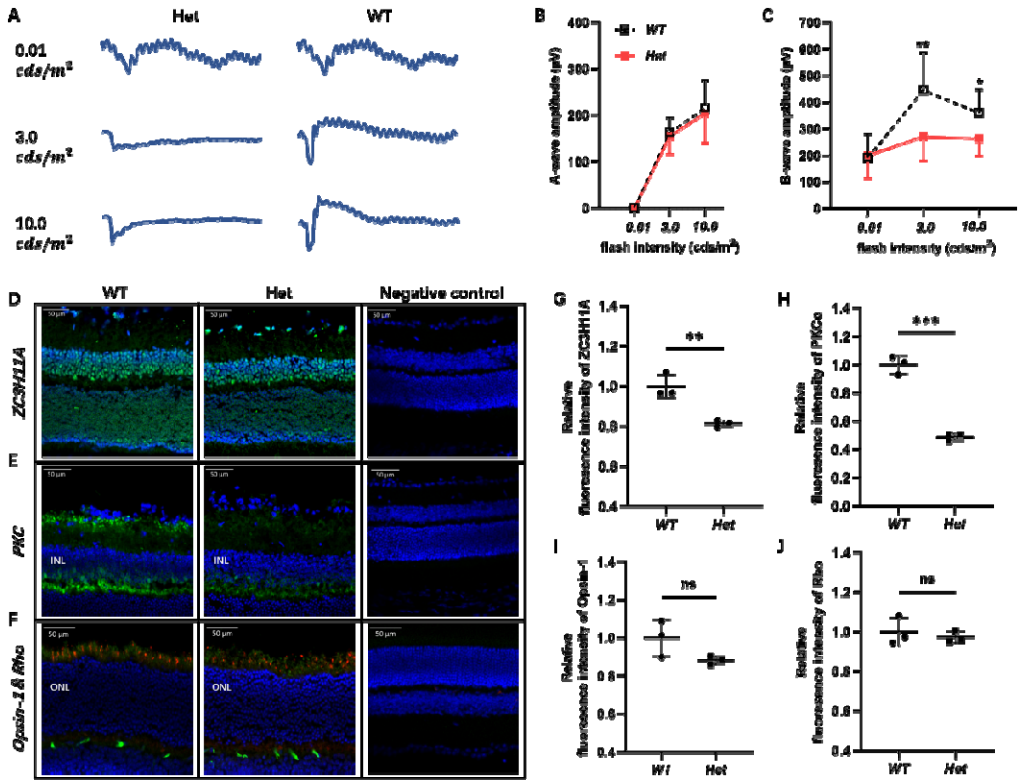

Figure 3. Electroretinography and immunohistochemical localization of Zc3h11a, PKCα, Opsin-1 and Rhodopsin in WT and Het-KO mice eyes. (A) Representative scotopic ERG responses from Het-KO and WT eyes at dark 0.01, 3.0 and 10.0 cds/ . (B, C) Statistical analysis of a-wave and b-wave amplitudes. Mean ± standard deviation, n=12/group. (D-F) Immunofluorescence-stained samples to detect Zc3h11a, bipolar cells, cone and rod cells. (G, H) Lower levels of Zc3h11a and PKCα (E. H) expression were observed in Het-KO mice (I, J) the expression levels of Opsin-1 and Rhodopsin between Het-KO and WT mice. Statistical significance was defined as *P < 0.05, **P<0.01 and ***P<0.001, as determined by independent samples t-tests.

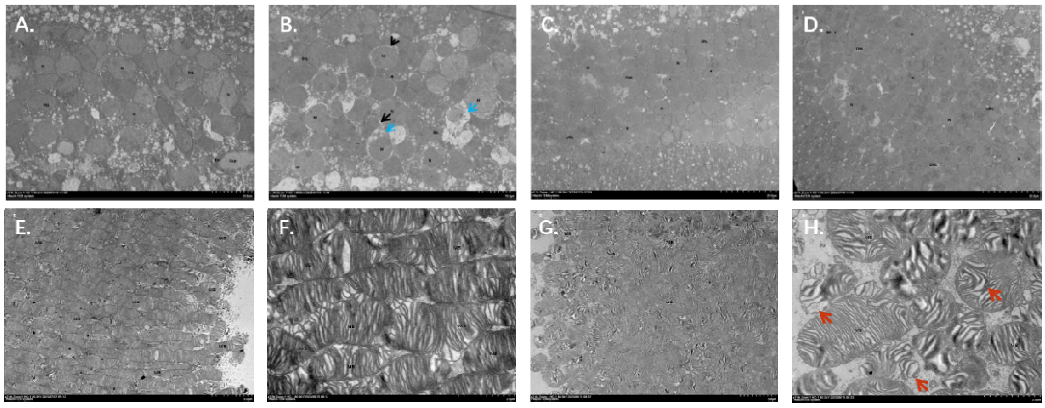

Figure 4. TEM showing the retinal ultrastructure of WT and Het-KO mice. (A, B) Cellular morphology of the INL in which bipolar cells are located in WT (A) and Het-KO mice (B). (C, D) Cellular morphology of the ONL in which the optic cells are located in WT (C) and Het-KO mice (D). (E, F) MB structure in WT mice. (G, H) MB structure of Het-KO mice.

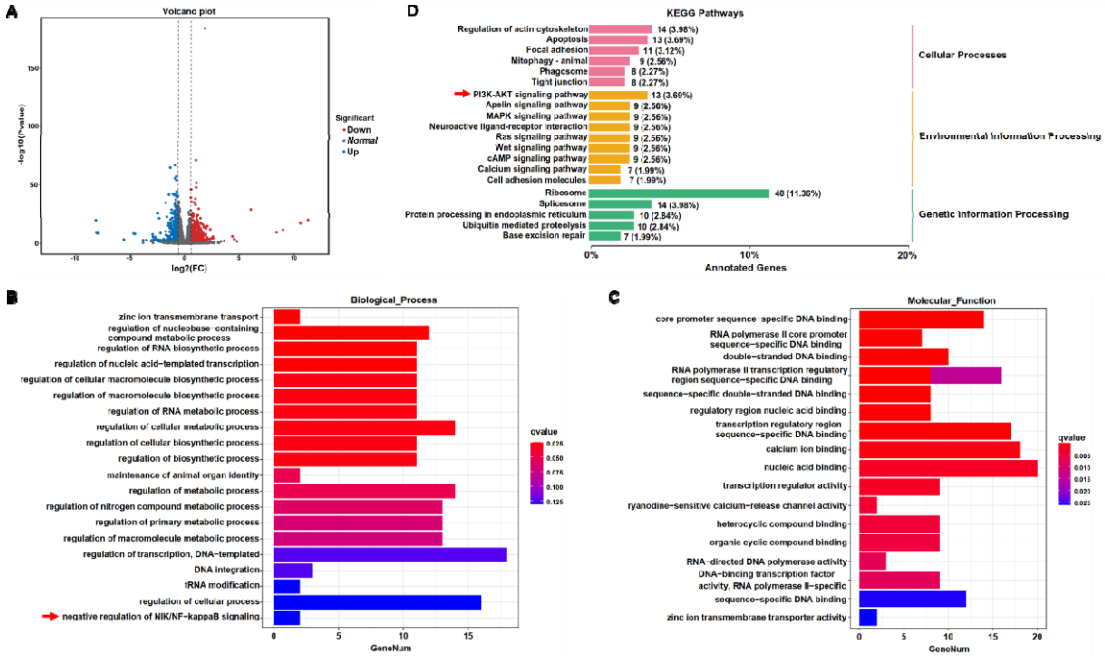

Figure 5. RNA-Seq analysis of molecular and pathway differences between WT control and Het-KO retinas. (A) Volcano maps were utilized to visualize the differentially expressed genes (DEGs) between WT control and Het-KO mouse retinas. (B, C) GO enrichment analysis of DEGs in the Het-KO group. (D) KEGG pathway enrichment analysis of DEGs in the Het-KO group.

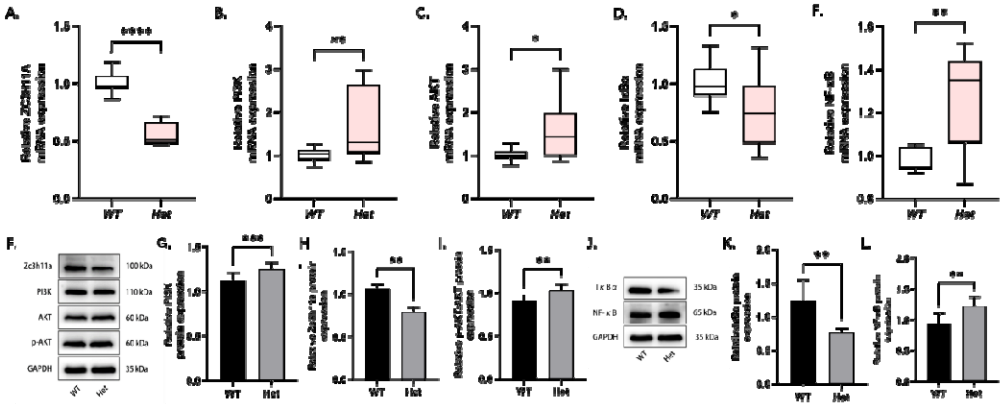

Figure 6. Effect of Zc3h11a on the expression of genes and proteins related to the PI3K-AKT and NF-κB signaling pathways in the retina. (A-C) The ZC3H11A, PI3K and AKT gene levels (n=3) were evaluated. (D, E) The IκBα and NF-κB gene levels (n=3). (F) Protein expression levels of ZC3H11A, PI3K, AKT, p-AKT and GAPDH were detected by western blot. (G-I) Quantitative analysis of the ZC3H11A and PI3K levels were normalized to GAPDH, while p-AKT levels were normalized to AKT (n=3). (J) The protein expression levels of IκBα, NF-κB and GAPDH were determined by western blot analysis. (K, L) Quantitative analyses of IκBα and NF-κB were normalized to GAPDH (n=3).

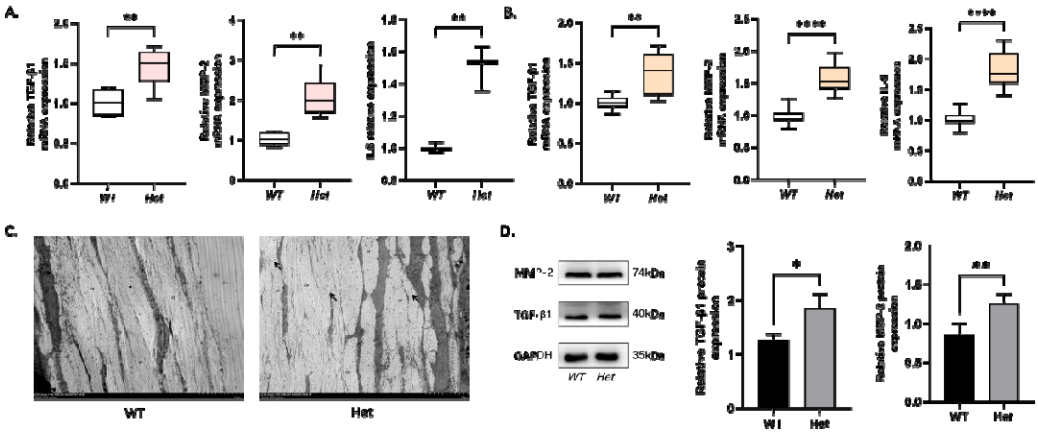

Figure 7. **Effect of Zc3h11a on the expression of TGF-β1, MMP-2 and IL-6 in the retina and sclera.** (A, B) Examination of TGF-β1, MMP-2 and IL-6 gene expression in the sclera (A) and retina (B) (n=3). (C) TEM structure of sclera. (D) Determination of TGF-β1 and MMP-2 protein expression levels, normalized to GAPDH, through western blot analysis (n=3).

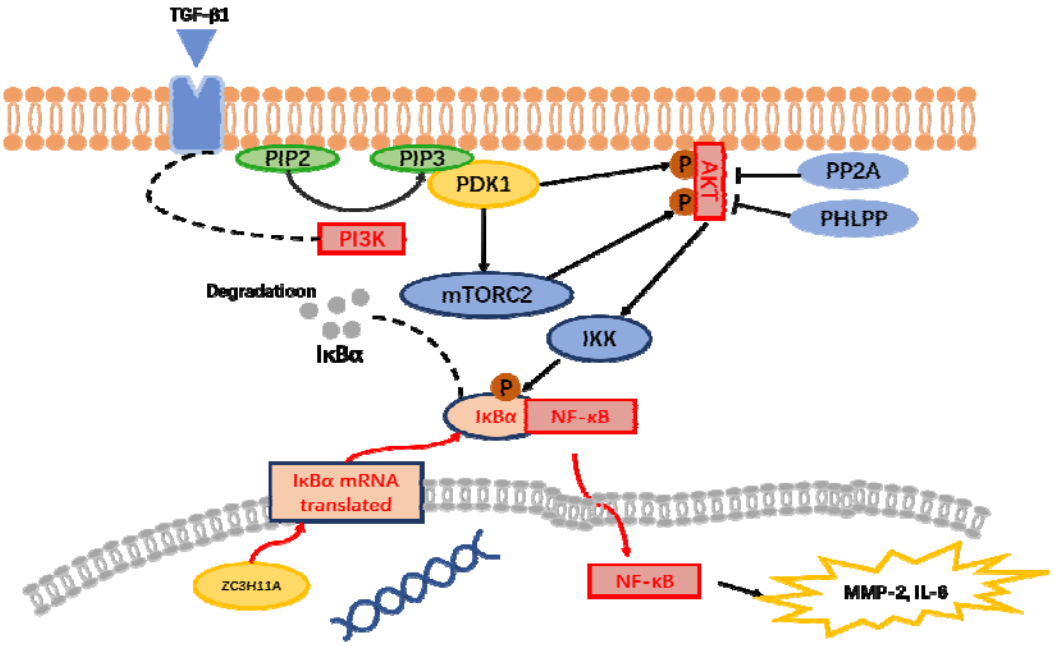

Figure 8. Schematic representation of the PI3K-AKT-NF-κB signaling pathway in retina.

Supplementary files

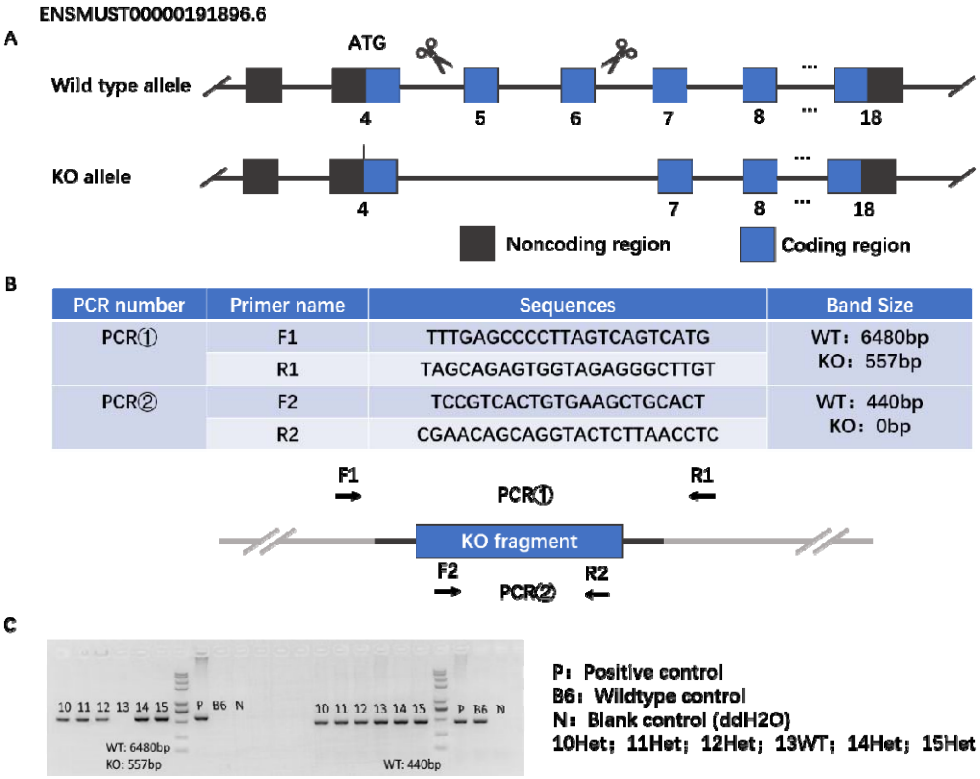

PCR number	Primer name	Sequences	Band Size
PCR①	F1	TTTGAGCCCCTTAGTCAGTCATG	WT: 6480bp KO: 557bp
	R1	TAGCAGAGTGGTAGAGGGCTTGT	
PCR②	F2	TCCGTCACTGTGAAGCTGCACT	WT: 440bp KO: 0bp
	R2	CGAACAGCAGGTACTCTTAACCTC	

Supplement Figure 1. Generation of Zc3h11a KO mice. (A) Generation of Zc3h11a KO mice in C57BL/6J background using CRISPR/Cas9 technology. (B-C) Primers for genotyping and examples of genotyping results of Zc3h11a Het-KO mice and wild-type mice

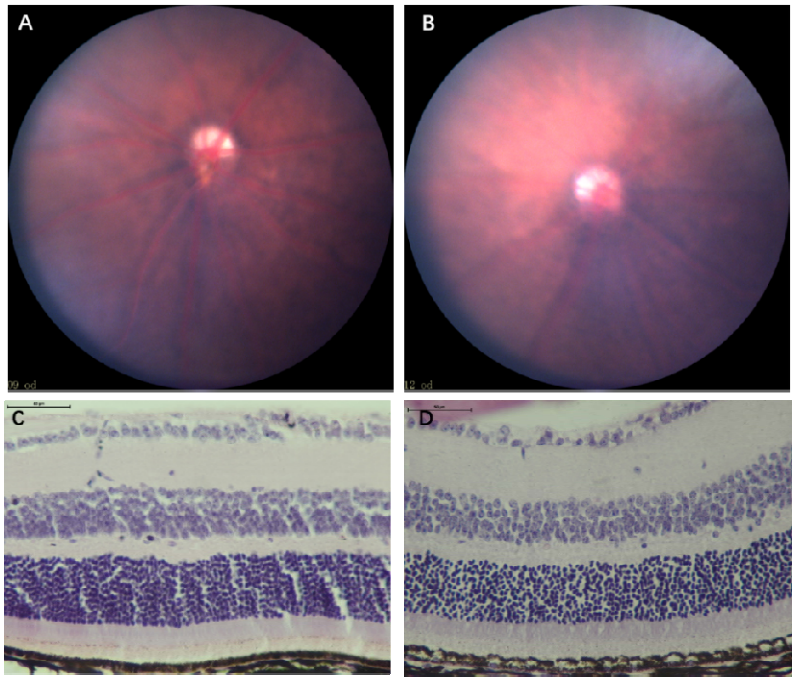

Supplement Figure 2. Fundus photographs and HE staining of Het and WT mice at 8th week. (A. B) Fundus photographs of WT (A) and Het-KO mice (B) (n=3). (C. D) HE staining of retina in WT (C) and Het-KO mice (D) (n=3).

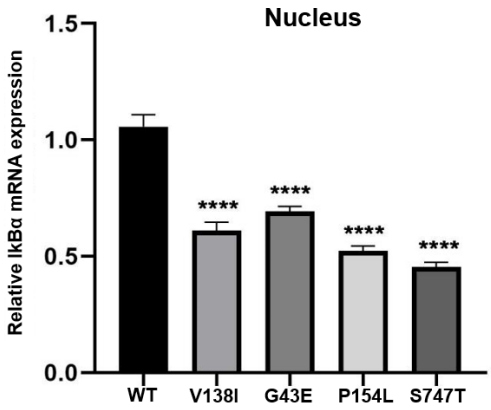

Supplement Figure 3. The relative mRNA expression levels of IκBα in the nucleus.

Supplementary Table 1. Sequence of oligonucleotides

Gene	Sequence
ZC3H11A	Forward: CTAAACTGCGCTTTCCATCACA Reserve: CGTTGATTACAACAGGCGGAT
PI3K	Forward: TGGGACCTTTTTGGTACGAGA Reserve: AGCTAAAGACTCATTCCGGTAGT
AKT	Forward: CCTTTATTGGCTACAAGGAACGG Reserve: GAAGGTGCGCTCAATGACTG
IκBα	Forward: TGAAGGACGAGGAGTACGAGC Reserve: TGCAGGAACGAGTCTCCGT
NF-κB	Forward: GGGGCCTGCAAAGGTTATC Reserve: TGCTGTTACGGTGCATACCC
TGF-β1	Forward: GTAACGCCAGCCAGGAATTGTTGCTA Reserve: CTTCAATACGTCAGACATTCGGG
IL-6	Forward: CTGCAAGAGACTTCCATCCAG Reserve: AGTGGTATAGACAGGTCTGTTGG
MMP-2	Forward: CAAGTTCCCCGGCGATGTC Reserve: TTCTGGTCAAGGTCACCTGTC
GAPDH	Forward: AGGTCGGTGTGAACGGCTTTG Reserve: TGTAGACCATCTAGTTGAGGTCA

The mRNA expression levels were analysed by the comparative $2^{-\Delta\Delta}$ Ct method and normalised using GAPDH.